Biophysical Journal
Article

Biophysical Society

Epithelial Monolayers Coalesce on a Viscoelastic Substrate through Redistribution of Vinculin

Ji Yun Zheng,[1,2] Siew Ping Han,[1,2] Yi-Jen Chiu,[1,2] Ai Kia Yip,[3] Nicolas Boichat,[2] Shi Wen Zhu,[2] Jun Zhong,[1,2] and Paul Matsudaira[1,2,*]

[1]Mechanobiology Institute of Singapore and [2]Center for BioImaging Sciences, Department of Biological Sciences, National University of Singapore, Singapore, Singapore; and [3]Biophysics Group, A*STAR Institute of High Performance Computing, Singapore, Singapore

ABSTRACT The mechanical properties of the microenvironment play a large role in influencing cellular behavior. In particular, the tradeoff between substrate viscosity and elasticity on collective cell migration by adherent cells is highly physiologically relevant, but remains poorly understood. To investigate the specific effects of viscous substrates, we plated epithelial monolayers onto polydimethylsiloxane substrata with a range of viscosities and elasticities. We found that on viscoelastic substrates the monolayers underwent rapid and coordinated movement to generate cell-free areas. To understand the molecular mechanism of this coordinated movement, we imaged various structural and signaling proteins at cell-cell and cell-matrix junctions. Through quantitative image analysis of monolayer disruption and subcellular protein redistribution, we show that the mechanosensor protein, vinculin, is necessary and sufficient for this viscous response, during which it is lost from focal adhesions and recruited by the cadherin complex to intercellular junctions. In addition, the viscous response is dependent upon and enhanced by actomyosin contractility. Our results implicate vinculin translocation in a molecular switching mechanism that senses substrate viscoelasticity and associates with actomyosin contractility.

INTRODUCTION

Cells continually sense and respond to mechanical cues from their microenvironment (1,2) through cell-cell and cell-matrix adhesions (3,4). One physical cue is viscoelasticity of the matrix to mechanical stress by cells and tissues (5–9). Elastic materials respond to applied force by storing and later releasing strain energy, whereas viscous materials dissipate force by undergoing flow. Therefore, the force profile of cell-substrate interactions might differ greatly for cells grown on viscous compared to elastic substrata. Although the effects of substrate elasticity on cellular function are well studied, the cellular response to viscosity has remained mostly unexplored. Cameron et al. (10,11) showed that changes to substrate viscosity affected the morphology, expression, and differentiation patterns of human mesenchymal stem cells. Earlier work from our lab has demonstrated that the collective movement of cells within epithelial sheets exhibited a critical transition from short-range to long-range correlated cell movement when the viscous and elastic moduli are equal (8). At this transition, cell traction forces can be transmitted over longer distances through strain in viscoelastic substrate than on an elastic substrate and thus mechanically coordinate longer-range collective movements such as epiboly during early development or movement on a thin basement membrane. Interestingly, although the viscoelasticity of the substrate should involve cell-matrix adhesions, both studies implicated cross talk to cell-cell adhesions by cadherins in the collective response to viscosity. However, the molecular details of how mechanical and chemical cues from the cell-substrate interface regulate cadherins at cell-cell interfaces were not investigated.

How could cadherin mediate collective cell motion through sensing stiffness of the substratum? The primary interface between cells and a viscoelastic substrate, and the best-understood cellular mechanosensing system to date, is the focal adhesion (FA). FAs have been well characterized as stiffness sensors, in which integrin receptors transmit information about the substrate matrix to the cellular interior and activate mechanosignaling pathways that regulate cellular proliferation, differentiation, and survival (12,13). Similarly, cadherin complexes can act as a mechanosensor that receives mechanical inputs from forces

Submitted February 14, 2017, and accepted for publication July 26, 2017.

*Correspondence: dbsmpt@nus.edu.sg

Ji Yun Zheng and Siew Ping Han contributed equally to this work.

Editor: James Sellers.

http://dx.doi.org/10.1016/j.bpj.2017.07.027

transmitted across intercellular junctions between neighboring cells (14–16). Although they have distinct subcellular locations, forces exerted at FAs and cadherin complexes are correlated with each other to maintain a constant total cellular tension (17,18). How this exquisite level of mechanical coupling is achieved is still poorly understood.

Chemical and mechanical cross talk between FAs and cadherin complexes could be mediated by a variety of mechanisms involving the actomyosin network, signaling pathways, or shared structural components (19), such as the mechanosensitive protein, vinculin. Vinculin localizes to, and in turn coordinates, FA composition in a force-dependent manner (20). Under tension, vinculin adopts an extended conformation that exposes multiple binding sites for many proteins associated with FAs or cadherin complexes (21–23). Similarly, junctional tension regulates the recruitment of vinculin to cadherin complexes by α-catenin, which is necessary for strengthening of E-cadherin-based junctions (24–26). Vinculin's key roles in both FA and cadherin complex dynamics identifies vinculin as a potential central regulator of FA-cadherin coupling (27,28).

In this study, we demonstrate that epithelial monolayers respond to substrate viscoelasticity by reorganizing cell-matrix and cell-cell adhesions, which involves cadherin-mediated recruitment of vinculin away from focal adhesions. The directed localization of vinculin to cell-cell adhesions, in combination with fibronectin reorganization and FAK-mediated actomyosin contractility, is implicated in regulating coordinated movement of epithelial monolayers.

MATERIALS AND METHODS

Cell culture

Cells were maintained in DMEM media supplemented with 10% fetal bovine serum and antibiotic-antimycotic (all from Life Technologies, Carlsbad, CA) at 37°C and 5% CO_2. CL-S1 cells were used between passages 26 and 32. Cells were plated onto fibronectin-coated polydimethylsiloxane (PDMS) substrata at 5–7.5 $\times$ 10^4 cells in a 100 μL drop and allowed to settle for 1 h, during which they formed a confluent monolayer at the base of the drop. In the case of MDCK cells, cells were allowed to settle for 2 h. After settling, 2–3 mL of media was added to the dish.

Plasmids

Plasmids encoding GFP-vinculin and GFP-αcat were gifts from Alpha Yap's lab (24). Plasmids encoding αcat-VH and αcat-VT were also gifts from Alpha Yap's lab (29) and subsequently cloned with GFP tag to get GFP-αcat-VH and GFP-αcat-VT. Plasmid encoding GFP-VT was synthesized by GenScript Biotech (Piscataway, NJ). The sequence of VT construct and pEGFP-C1 vector were provided in the Supporting Material.

PDMS substrate

We imaged the dynamics of confluent cells on PDMS substrates. Viscoelastic, soft elastic, and elastic substrata were prepared by mixing cross-linker and polymer (Sylgard 184; Dow Corning, Midland, MI) at ratios of 1:80, 1:60, and 1:20, respectively. The mixtures were degassed and spin-coated (6000 RPM for 10 s) onto 35-mm standard dishes (Corning, Tewksbury, MA) or imaging dishes (Ibidi, Martinsried, Germany), which were baked at 80°C for 2 h. The resultant PDMS substrata were 20–30 μm thick. For imaging procedures, a 100 μL drop of 20 μg/mL fibronectin from bovine plasma (Sigma-Aldrich, St. Louis, MO) was then adsorbed to the PDMS at room temperature for 1 h. This resulted in a circle of $\sim$5 mm diameter within which epithelial cells could attach. For protein extraction procedures, the entire base of the dish was coated with fibronectin.

The shear modulus of PDMS was measured by a rheometer with a temperature-controlled plate in a 25-mm cone and plate (0.04 rad) geometry (Advanced Rheometric Expansion System; TA Instrument, New Castle, DE) at 37°C with 1% strain and a frequency sweep between 0.1 and 100 rad/s. The characteristic modulus was taken at 1 rad/s.

Fabrication of polyacrylamide substrates

To image displacements of the substrate, we prepared fluorescent bead-embedded polyacrylamide (PA) substrates following previously published protocols (3,6). Briefly, to activate the glass surface for PA attachment, the 25-mm diameter coverslips were pretreated with 3-aminopropyltrimethoxysilane (Sigma-Aldrich) for 5 min and washed with distilled water twice, for 5 min each time. A quantity of 0.5% glutaraldehyde (Sigma-Aldrich) in phosphate-buffered saline was then added to the coverslips for 30 min, rinsed twice with distilled water, and then left to dry.

To fabricate PA substrates of varying storage (G') and loss (G'') modulus, acrylamide (Bio-Rad, Hercules, CA) and bisacrylamide (bis; Bio-Rad) were mixed in different ratios following the values published in (7). The soft elastic substrates (SE; $G' = 4.94 \pm 0.49$ kPa, $G'' = 1 \pm 0.1$ Pa) were prepared with 8% acrylamide: 0.1% bis, whereas the viscoelastic substrates (VE; $G' = 4.73 \pm 0.47$ kPa, $G'' = 10 \pm 1$ Pa) were prepared with 12% acrylamide: 0.0358% bis (values obtained from (7)).

A 1/25 volume of 0.2-μm diameter red fluorescent beads (excitation and emission wavelength of 580 and 605 nm, respectively; Invitrogen, Carlsbad, CA) were added to the prepolymerized acrylamide-bis mixture. Polymerization of the acrylamide-bis mixture was initiated with 1:100 volume of 10% ammonium persulfate (Bio-Rad) and 1:1000 volume N,N,N′,N′-Tetramethylethylenediamine (Bio-Rad). A quantity of 5 μL of the prepolymerized solution was placed onto the pretreated 25-mm-diameter glass coverslip, and covered with another untreated 12-mm-diameter circular coverslip. After 15 min when the substrates have polymerized, the top coverslips were carefully removed and substrates were rinsed with 50 mM HEPES, pH 8.5.

The PA substrates were coated with 50 μg/mL fibronectin using 0.5 mg/mL sulfo-succinimidyl-6-(4-azido-2-nitrophenyl-amino) hexanoate (sulfo-SANPAH; Pierce, Rockford, IL) in HEPES. The substrates were covered with the sulfo-SANPAH solution and exposed to UV light in a sterile hood for 15 min. The substrates were then washed with HEPES for 15 min, covered by 50 μg/mL fibronectin (Sigma-Aldrich) at room temperature for 2 h on a rocker, rinsed with phosphate-buffered saline, and then sterilized by exposure to UV light in a sterile hood for 15 min. The substrates were then allowed to incubate for 30 min in cell culture medium at 37°C before cells were plated.

Measurement of bead displacements within the PA substrates

To measure the bead displacements caused by a single cell, cells were imaged on fibronectin-coated bead-embedded PA substrata on an A1R+ confocal microscope (Nikon, Melville, NY) with a 60$\times$ oil objective lens (N.A. 1.4) 12 h postsettling. For each data point, a differential interference contrast image of the cell and a fluorescence image of the beads embedded within the PA substrates was acquired. Cells are then detached from the

substrate after adding 0.5% (wt/vol) SDS detergent for 10 min, and another fluorescence image of the beads was obtained to determine the bead locations in the unstrained substrate.

The bead displacements on the strained substrate caused by the cells were calculated by comparing with the bead positions in the unstrained substrates, following the digital image correlation algorithm as mentioned in the above section and detailed in (3).

Antibodies and immunostaining

The following primary antibodies were used: Mouse anti-FAK (immunofluorescence (IF) 1:400, Western blotting (WB) 1:5000), mouse anti-fibronectin (IF 1:100), mouse anti-E-cadherin (WB 1:1000), and mouse anti-paxillin (IF 1:200), all from BD Biosciences, Franklin Lakes, NJ; rabbit anti-vinculin (IF 1:500, WB 1:1000), rat anti-E-cadherin (IF 1:500), phalloidin-647 for F-actin staining (IF 1:500), and Hoechst for nucleus staining (1 μg/mL), all from Life Technologies; mouse anti-vinculin (IF 1:400), mouse anti-β-actin (WB 1:2000), and rabbit anti-α-catenin (WB 1:2000), all from Sigma-Aldrich; rabbit anti-phospho-FAK (Tyr^{397}, IF 1:50, WB 1:500), rabbit anti-MLC (IF 1:50, WB 1:500), and rabbit anti-phospho-MLC (IF 1:50, WB 1:500), all from Cell Signaling Technology, Danvers, MA; rabbit anti-myosin IIb (IF 1:100; Thermo Fisher Scientific, Waltham, MA), rabbit anti-N-cadherin (IF 1:100, WB 1:1000), rabbit anti-myosin IIa (IF 1:100), and rat anti-$\alpha 5\beta 1$ (IF 1:100), all from Abcam, Cambridge, MA.

The following secondary antibodies and dyes were used for immunocytochemistry: goat anti-mouse Alexa Fluor 488 (1:500), goat anti-rabbit Alexa Fluor 568 (1:500), donkey anti-rat AlexaFluor 568 (1:500), and phalloidin Alexa Fluor 568 (1:500), all from Life Technologies; and Hoechst 33342 (Sigma-Aldrich).

The following secondary antibodies were used for Western blotting: goat anti-rabbit HRP conjugate (1:2000) and goat anti-mouse HRP conjugate (1:2000), both from Bio-Rad.

Drug treatment

All stock solutions were prepared in DMSO. Cells were treated with FAK inhibitor PF-562271 (Selleck Chemicals, Houston, TX) and MMP inhibitor GM6001 (Millipore, Billerica, MA) during and after settling, and imaged 6 h posttreatment. Cells were treated with blebbistatin, cytochalasin D, and RhoK inhibitor Y27632 (all from Sigma-Aldrich) after settling and then imaged 4 h posttreatment. CL-S1 cells were treated with Calyculin A (Cell Signaling Technology) at 1 h postsettling and imaged 2 h posttreatment.

MMP assay

2×10^6 CL-S1 cells were plated onto 35 mm dishes coated with PDMS and fibronectin across the entire base. At 1 h postsettling, the media was removed and 1 mL of fresh culture media was added. After another hour, the culture media was collected and assayed using a Sensolyte 520 Generic MMP Assay Kit (AnaSpec, Fremont, CA), and the readout was measured on an Infinite M200 Reader (Tecan, Männedorf, Switzerland).

Transfection

Transfections of CL-S1 cells were performed by electroporation (Neon Transfection System; Life Technologies). Transfections of MDCK cells were performed using Lipofectamine 2000 (Life Technologies). The following SMARTpool (GE Dharmacon, Lafayette, CO) siRNAs were used: L-040206-00-0005 (N-cadherin), L-048960-01-0005 (α-catenin), L-060130-01-0005 (vinculin), and D-001810-01-05 (control).

Live cell imaging

Cells were imaged at 0 h postsettling in the phase contrast channel on a BioStation IM-Q (Nikon) for 3–12 h. Images at single time points were also taken for drug treatment or transfection experiments.

For quantitation of cell-free area, images were acquired every 15 min. 3×3 panels of images were stitched using an ImageJ plugin (National Institutes of Health, Bethesda, MD) (30) to generate a final area of $\sim 2 \times 1.5$ mm. Stitched images were then passed through a variance and threshold filter to segment and measure the cell-free area in ImageJ.

Confocal microscopy

Immunostained fixed cells were imaged on a model No. LSM510 microscope (Carl Zeiss, Oberkochen, Germany) with an Apochromat 63× NA 1.4 oil immersion lens. Quantitative image analysis and image processing were performed using the software ImageJ and the software Imaris (Bitplane, Belfast, UK), respectively.

To quantify the proportion of vinculin in the junctional or focal adhesion pool, a mask was generated using the N-cadherin or paxillin channel, respectively. The mask was applied to maximum projections of the corresponding vinculin images. The percentage of vinculin in each pool was calculated as the fraction of vinculin within the mask region over total vinculin, i.e., vinculin $\cap$ mask/(vinculin $\cap$ mask + vinculin $\cap$ non-mask). The number and size of vinculin particles were measured using the Analyze Particles function of the software ImageJ.

Calculation of cell velocity and correlation

Phase contrast images of the cell monolayer measuring 882.5×706 μm (500×400 pixels) were obtained using the Biostation IM-Q (Nikon, Melville, NY) at 10× magnification at 3 min intervals.

Cell displacement fields were obtained by comparing the image intensities changes between each image sequence following a digital image correlation algorithm (1–3) implemented in MATLAB (The MathWorks, Natick, MA). Using a pair of corresponding subareas (Ω) of the images whose intensities are represented by $f(\boldsymbol{x})$ and $g(\boldsymbol{x})$ before and after being displaced by a displacement $\boldsymbol{u}$, respectively, the cross correlation function $m(\boldsymbol{u})$ that gives a measure of similarity between the two subareas was calculated:

$$m(\mathbf{u}) = \int f(\mathbf{x}) g(\mathbf{x}+\mathbf{u}) d\Omega_x. \quad (1)$$

The cross correlation function was efficiently obtained by applying the fast Fourier transform (FFT) algorithm and the displacement vector of the subarea between time intervals was estimated from the location of the cross correlation peak,

$$m(\mathbf{u}) = F^{-1}\{F[f(x)] * F[g(x)]\}, \quad (2)$$

where F, $*$, and F^{-1} denotes the FFT, the complex conjugate, and the inverse FFT, respectively.

The image drift between each time interval was first computed and corrected by defining the subarea Ω to be a 350×350 pixel window in the images. After correcting for image drift, the images were subsequently divided into smaller subareas Ω of window size 20×20 pixels (approximate area occupied by a cell) with 50% overlap and the displacement field of the cell movements between each time interval was calculated. The velocity field was obtained by dividing the displacements with the time interval (3 min).

The correlation length, over which cell movements were correlated, was calculated following previous publications (31,32). The correlation coefficients for the horizontal (C_u) and vertical (C_v) velocity components along

the x- and y axis, respectively, were calculated following the formulae below:

$$C_u(\vec{r}) = \left\langle \frac{\left\langle u^*\left(\vec{r'}+\vec{r},t\right) \times u^*\left(\vec{r'},t\right)\right\rangle_{\vec{r'}}}{\left[\left\langle u^*\left(\vec{r'}+\vec{r},t\right)^2\right\rangle\left\langle u^*\left(\vec{r'},t\right)^2\right\rangle\right]^{1/2}}\right\rangle_t, \quad (3a)$$

$$C_v(\vec{r}) = \left\langle \frac{\left\langle v^*\left(\vec{r'}+\vec{r},t\right) \times v^*\left(\vec{r'},t\right)\right\rangle_{\vec{r'}}}{\left[\left\langle v^*\left(\vec{r'}\right)(+\vec{r},t)^2\right\rangle\left\langle v^*\left(\vec{r'},t\right)^2\right\rangle\right]^{1/2}}\right\rangle_t, \quad (3b)$$

where u^* and v^* represent the deviation of the velocity from the mean velocity in the x- and y axis, respectively; and t refers to the time point. $\vec{r'}$ represents the coordinates of a point and $\vec{r}$ represents the distance of another point where correlation was computed. The correlation coefficients were averaged over all time points, and a graph of $log\ C_u$ (or $log\ C_v$ for vertical velocity component) versus distance $|r|$ was fitted to a straight line. The correlation length, which is a characteristic length scale of correlation, was obtained by taking the inverse of the gradient of the fitted straight line.

Fluorescence recovery after photobleaching

Fluorescence recovery after photobleaching (FRAP) of cells expressing GFP-vinculin was performed on an UltraviewVox (Perkin Elmer, Waltham, MA) with a UPLSAPO 60× NA 1.2 water immersion lens (Olympus, Melville, NY). An area of 20 × 20 pixels was bleached with the 405 and 488 lasers at 100% power. Images were acquired for 5 s prebleach and 100–300 s postbleach at a rate of 100 frames per s, and movies were analyzed using the software Volocity (Perkin Elmer).

RESULTS

Epithelial cell monolayers coalesce in response to substrate viscoelasticity

We had previously shown that on viscous and viscoelastic PDMS, a confluent monolayer of CL-S1 cells displays a cadherin-dependent and highly correlated cell migration (8) that led to coalescence of cells into a 3D aggregate. To extend these studies, we initially investigated the longer-term effect of substrate viscoelasticity on the integrity of the monolayer dynamics. First, to establish the reproducibility of the Murrell coalescence assay, we confirmed that on a VE substrate ($\zeta = 0.0125$, 1:80 cross-linker ratio, Fig. S1 *A*) and over the course of several hours, a confluent monolayer of CL-S1 cells initially moved in a correlated motion (data not shown) that over a longer period led to coalescence into dense aggregates (Movie S1). Coincident with coalescence is the simultaneous emergence of small cell-free areas that enlarged throughout the entire monolayer (Movie S1). Next, we tested whether coalescence is an artifact of cell death and not a result of strain-induced movement. However, we found that the cells around emerging and existing cell-free areas (Movie S2) took up calcein (a live cell labeling dye), thus ruling out the monolayer being disrupted by local cell death. To test whether coalescence is a general response on VE substrates, we compared coalescence on VE substrates by epithelial and nonepithelial cells (Fig. 1 *A*). We found that HeLa and IEC6 cells also coalesced, demonstrating that it is not unique to CL-S1 cells, whereas in contrast, MDCK and NIH3T3 monolayers remained confluent over the same period. Furthermore, there was no correlation between the occurrence of cell coalescence and the type of cadherin expressed because whereas HeLa and NIH3T3 cells express only N-cadherin and MDCK and IEC6 cells express only E-cadherin, CL-S1 cells express both (Fig. 1 *B*). Because the cell-free area was simpler to quantify than correlated motion, our measurements showed that CL-S1 cells exhibited the fastest rate and greatest extent of coalescence (Fig. 1, *C* and *C′*) compared to the other cells, and therefore this cell line was selected for further experimentation.

To confirm that correlated movement leading to coalescence is linked to the viscous properties of the substrate, we compared the extent of coalescence on VE, soft elastic (SE), and elastic (E) substrata and observed cell coalescence on VE substratum, but not on SE or E substrates (Fig. 1, *D–E′*; Movie S3). On viscoelastic substrates, where the viscous moduli and elastic moduli are of similar magnitude, cell coalescence appeared by 6 h and grew to large cell-free areas by 12 h (Fig. 1 *D*). In contrast, there was no difference in coalescence levels on SE and E substrata (Fig. 1 *E′*) whose elasticity differs by two orders of magnitude (Fig. S1 *A*). Moreover, consistent with our previous findings (8), when viscous moduli are larger than elastic moduli, the correlated motion is further elevated as the contraction of the tissue drives the substrate to flow (Movie S4). Hence, the effect of VE substrata is primarily due to its high viscosity rather than its low elasticity.

Because coalescence is an endpoint of correlated motion, we compared the correlated motion of CL-S1 cells on different substrata with that of MDCK cells, which do not undergo coalescence (Fig. 1, *A–C′*). Our measurements showed that the correlation lengths in x and y are highest for CL-S1 cells on VE substrate and half the VE values on soft elastic and elastic substrata. Although MDCK cells do not coalesce, we detected they exhibit correlated movement that was comparable on all three substrata at values similar to the CL-S1 cells on E and SE (Fig. 1, *F* and *F′*). These results not only confirm previous studies that correlated movement by CL-S1 cells is enhanced on viscoelastic substrates, but—most interestingly—suggest that MDCK can initiate correlated movement but not complete coalescence.

Cell coalescence perturbs cell-matrix organization

We previously demonstrated that viscous and viscoelastic substrates yield as cells begin to coalescence (8) and that

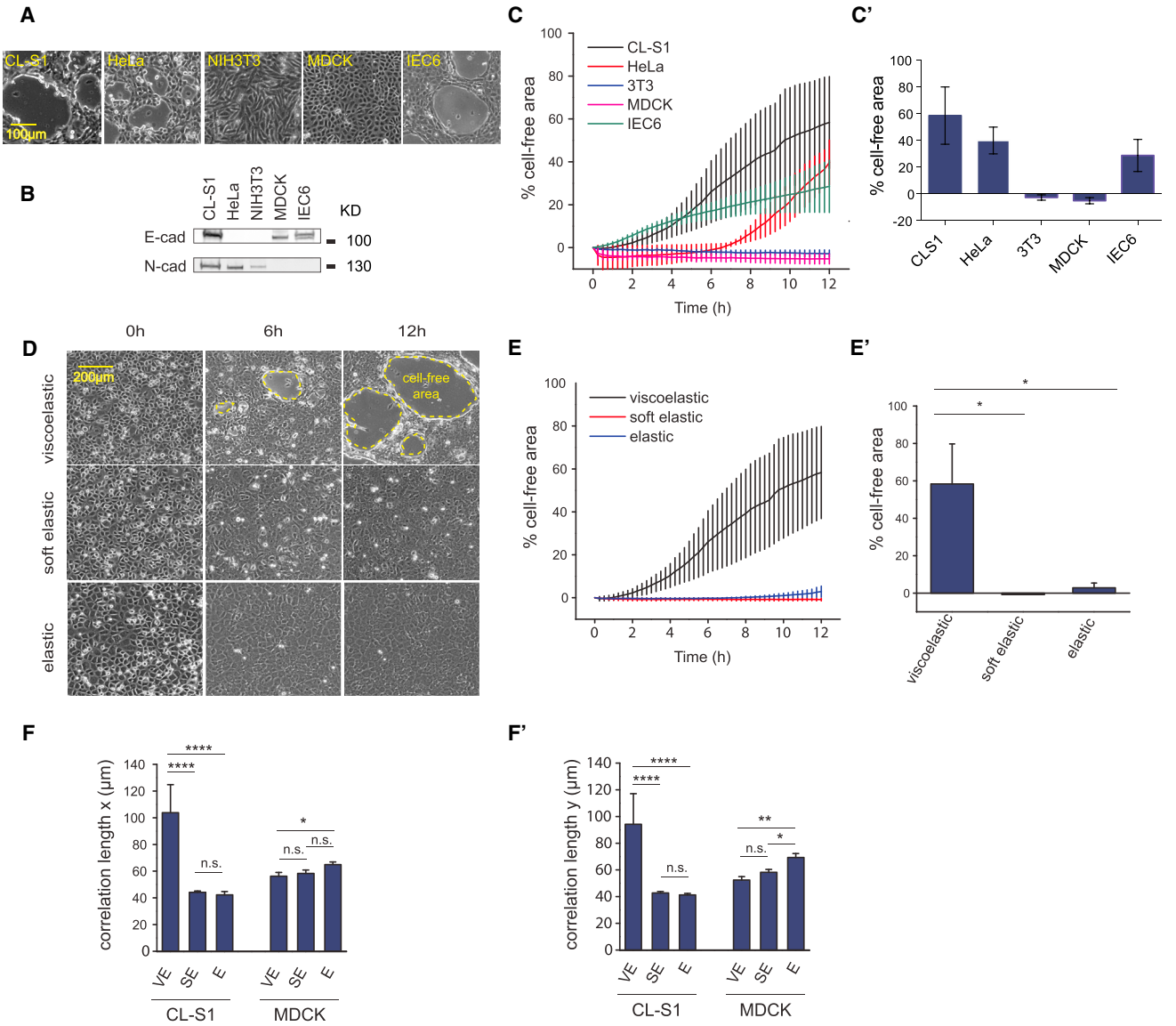

FIGURE 1 Substrate viscoelasticity induces cell coalescence. (*A*) Given here is a comparison of cell-free areas in confluent cultures of CL-S1, HeLa, NIH3T3, MDCK, and IEC6 cells grown on viscoelastic PDMS. (*B*) Given here is Western blot of whole cell lysates of CL-S1, HeLa, NIH3T3, MDCK, and IEC6 cell lines, immunoblotted for E- and N-cadherins. (*C*) Shown here is a graph of the development of cell-free area in confluent cultures of CL-S1 (*black*), HeLa (*orange*), NIH3T3 (*blue*), MDCK (*red*), and IEC6 (*green*) cells ($n = 3$–4), on VE PDMS. (*C′*) Given here is the extent of cell coalescence on VE PDMS in different cell lines at 12 h postsettling. Values correspond to 12 h endpoint in (*C*). (*D*) CL-S1 cells on VE, SE, and E PDMS substrata are shown under a wide-field microscope. Panels correspond to 0 h (*left column*), 6 h (*middle column*), and 12 h (*right column*) time points ($n = 3$–4). (*E*) Shown here is a graph of increase in cell-free area in CL-S1 monolayer over time on elastic (*blue*), soft elastic (*red*), and viscoelastic (*black*) PDMS substrata. The viscoelastic curve is from the same data as the CL-S1 cell coalescence data in (*C*). (*E′*) The extent of cell coalescence was significantly reduced on SE and E PDMS substrata compared to VE PDMS substrate at 12 h postsettling. (*F* and *F′*) Correlation of cell movement in the *x* direction (*F*) and *y* direction (*F′*) was calculated from PIV analysis of movies of CL-S1 and MDCK cells on VE, SE, and E PDMS substrata. $*p < 0.05$, $**p < 0.01$, $****p < 0.0001$; n.s., not significant; bars represent SE.

a cell-generated force was transmitted through the matrix because the fluorescent collagen appeared strained at the onset of coalescence. If a traction force originates from the cell, then we might detect changes in the organization of matrix and adhesion proteins. To test this idea, we reinvestigated whether a fibronectin matrix is similarly perturbed in a cell coalescence assay and determined whether matrix protease activity is detected during coalescence. Immunostaining of fibronectin-coated substrata without cells attached demonstrated that the coating was homogenous and consistent across VE, SE, and E substrata (Fig. S1, *B* and *C*). Immunostaining of fixed cells showed that cell-free areas were devoid of fibronectin, which appeared to have been detached from the substrate by the retreating

cell front (Fig. 2 *A*, *top two panels*). On VE substrate, fibronectin within the intact monolayer was concentrated in fibrillar structures localized basal to intercellular junctions, and depleted in the regions underneath the cell body (Fig. 2 *A*, *middle panel*). In contrast, fibronectin was less perturbed and remained more evenly distributed on SE and E substrata (Fig. 2 *A*, *bottom two panels*). This pattern of immunostaining was also present in HeLa cells (Fig. S1 *D*) and, to a lesser extent in MDCK cells (Movie S5). Consistent with the data from fixed samples, live cell imaging of monolayers plated onto fluorescently labeled fibronectin showed that disruption of fibronectin was most pronounced on VE substrate, with fibronectin-free patches and fibrillar structures appearing from the start of imaging (Movie S6). The fibronectin fibrils formed on VE substrate colocalized with integrin clusters to a significantly greater degree than on SE and E substrata (Fig. 2 *B* and *B′*). This suggested that substrate viscoelasticity can induce intracellular changes in the organization of adhesion proteins in addition to the marked perturbation of extracellular matrix.

To address whether the matrix organization is perturbed by matrix proteases, we measured the metalloprotease activity in the media from CL-S1 monolayers grown on the various substrata. Comparison of protease activity showed only small differences in MMP activity (Fig. 2 *C*), and this was not correlated with coalescence. Furthermore, when metalloproteases are inhibited by MMP inhibitor, GM6001, cell coalescence was not affected (Fig. 2 *D*). Thus, the observed changes in matrix organization cannot

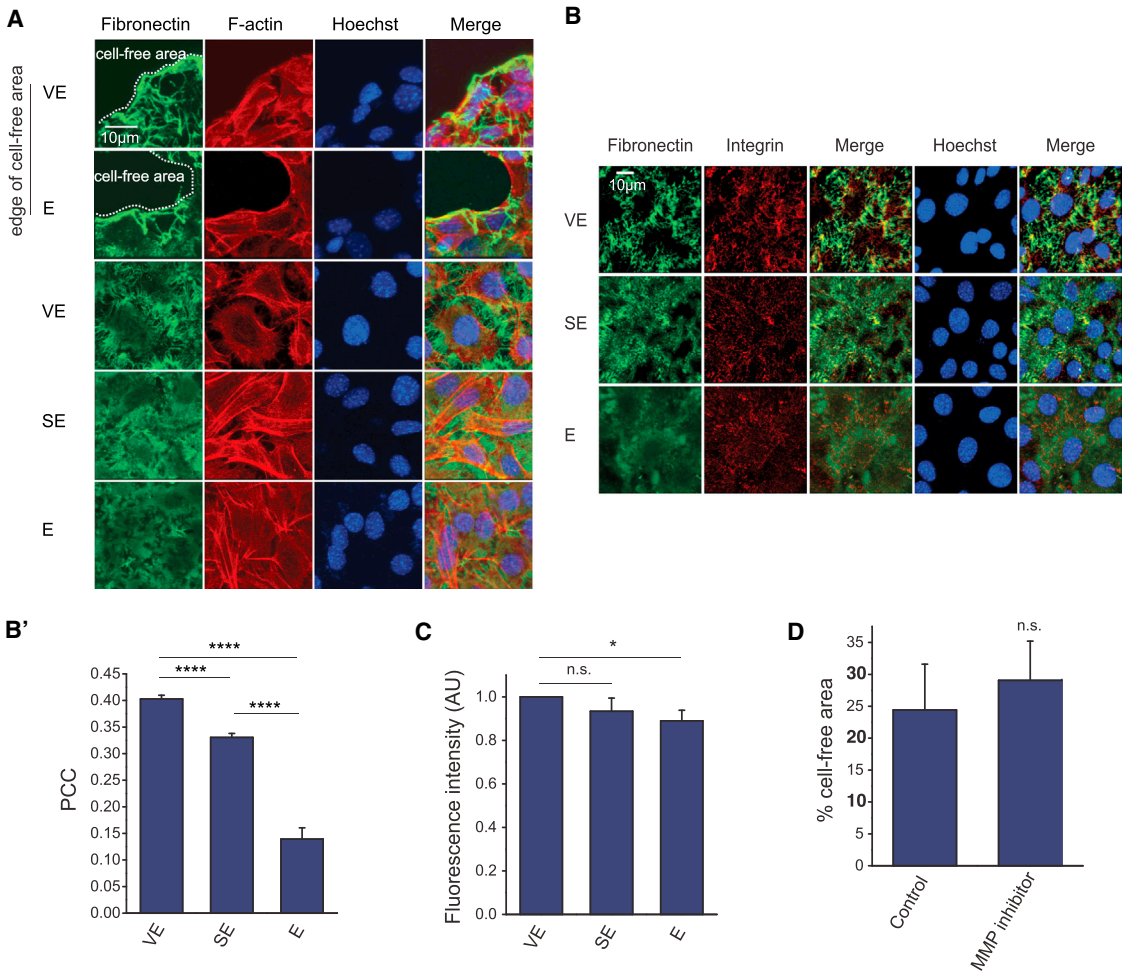

FIGURE 2 Effect of substrate viscoelasticity on cell-matrix interactions. (*A*) Given here are confluent CL-S1 cells grown on VE, SE, and E PDMS substrata, fixed at 4 h postsettling and stained to visualize fibronectin, F-actin, and nucleus. (*B*) Confocal images of CL-S1 cells are shown on different PDMS substrata fixed and immunostained for fibronectin, integrin, and nucleus, 4 h postsettling. (*B′*) Given here is quantitative image analysis on the colocalization between fibronectin fibrils and integrin clusters using Pearson's correlation coefficient (*PCC*) ($n = 6$). (*C*) Media overlaying CL-S1 monolayers on different PDMS substrata were collected 1 h postsettling and MMP activity was measured by a *Förster resonance energy transfer*-based assay, in which higher fluorescent readouts corresponded to higher activity levels ($n = 5$). (*D*) CL-S1 monolayers on VE PDMS were treated with MMP inhibitor (25 nM GM6001) and the cell-free area was measured 4 h postsettling. MMP inhibition had no significant effect on cell coalescence ($n = 7$). *$p < 0.05$, ****$p < 0.0001$; n.s., not significant; bars represent SE. To see this figure in color, go online.

be attributed to fibronectin breakdown, and instead, are likely to result from physical disruption by cellular movement.

A final control experiment addressed whether the cross-linker ratio of PDMS can influence fibronectin adsorption (33) through differences in hydrophobicity or surface roughness. To evaluate this parameter, we compared coalescence on thick-versus-thin PDMS substrata. Both substrates have identical chemical and topological roughness but differ in apparent stiffness because a thin substrate is dominated by the stiffness of the underlying plastic dish. We found that cell coalescence occurred on thick but not thin VE substrate (Fig. S1 *E*). Moreover, fibronectin was also less perturbed on thin substrate (Fig. S1 *F*). Taken together, these results demonstrated that coalescence is dependent on the mechanical, rather than chemical, properties of the substrate.

Substrate viscoelasticity extends the range of cell-substrate forces

Next, we sought to determine whether the physical properties of VE substrate could directly contribute to cell coalescence, by tracking substrate surface displacements caused by single cells. As tracker beads did not disperse evenly in hydrophobic PDMS, soft elastic and viscoelastic PA gels were used instead (10). Analysis of bead displacement showed that forces exerted by CL-S1 cells distorted the substrate to a larger extent and over a greater area on VE compared to SE substrate (Fig. 3, *A*–*B′*). Furthermore, displacements were focused at cellular protrusions on SE substrate (Fig. 3, *A* and *A′*), whereas they extended continuously throughout the area beneath the cell and for a significant distance away from the cell on VE substrate (Fig. 3, *B* and *B′*). In agreement with previous studies (10), cells were slightly more spread on VE than SE substrate. However, because the bead displacement field extended over more than two cell areas, the long-range cell displacements are likely primarily due to the enhanced propagation of cellular forces through the substrate, rather than differences in cell-substrate interactions.

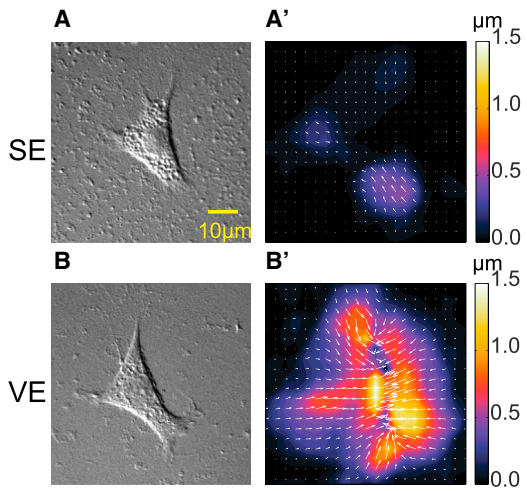

FIGURE 3 Cell-substrate forces propagate further on viscoelastic PA substrate. (*A* and *B*) Given here are differential interference contrast images of single CL-S1 cells on SE (*A*) and VE (*B*) PA gels embedded with fluorescent beads. (*A′* and *B′*) Shown here are heat maps of corresponding bead displacements due to cell traction forces. On SE PA gel, displacements were small and localized to cellular protrusions, whereas on VE PA gel, displacements extended throughout the cell and its surrounding regions. To see this figure in color, go online.

Coalescence is dependent upon FAK-mediated actomyosin contractility

To better understand the molecular basis for the cellular movement involved in cell coalescence, we tracked the positions of cells by particle image velocimetry (PIV) of coalescing CL-S1 monolayers (Fig. 4 *A*; Movie S7). We observed that the formation of cell-free areas was preceded by a sudden, transient, and coordinated movement of cells away from the eventual location of the cell-free area. This suggested that strain across the monolayer might be important in generating coalescence. To identify the source of the strain, CL-S1 monolayers on VE substrata were treated with chemical modulators of actomyosin contractility. We found that inhibitors of contractility reduced coalescence (Fig. 4 *B*), whereas treatment of monolayers with Calyculin A (a drug that enhances actomyosin contractility) had the opposite effect of increasing coalescence (Fig. 4 *C*). Notably, although Calyculin A treatment also increased coalescence in treated CL-S1 cells on SE and E substrata, the levels of coalescence did not reach the same extent of coalescence by the untreated control cells on VE substrata. Interestingly, Calyculin A treatment did not induce coalescence in MDCK cells (Fig. 4 *C*). These results suggest that coalescence is directly correlated with actomyosin contractility but remains restricted to a viscoelastic substrate.

We noted earlier that cell coalescence was also correlated with increased colocalization between integrin and fibronectin (Fig. 2 *B*), which might affect the function of other focal adhesion proteins. Focal adhesion kinase (FAK) is a downstream effector of integrin signaling that regulates actomyosin contractility (34). We found that drug inhibition of FAK led to a dose-dependent reduction in coalescence (Fig. 4 *D*). Furthermore, FAK inhibition prevented the increase in coalescence induced by Calyculin A treatment (Fig. 4 *E*). Therefore, coalescence involves a strain-producing mechanism mediated through FAK-actomyosin contractility.

However, measurement of p-FAK levels on different substrata by both Western blotting of whole cell lysate and immunostaining of fixed cells did not reveal any increase in FAK activity on VE substrata (Fig. 4, *F*–*G*). Furthermore, there were no obvious differences in p-MLC subcellular localization (Fig. 4 *H*) on different substrata, nor were myosin II

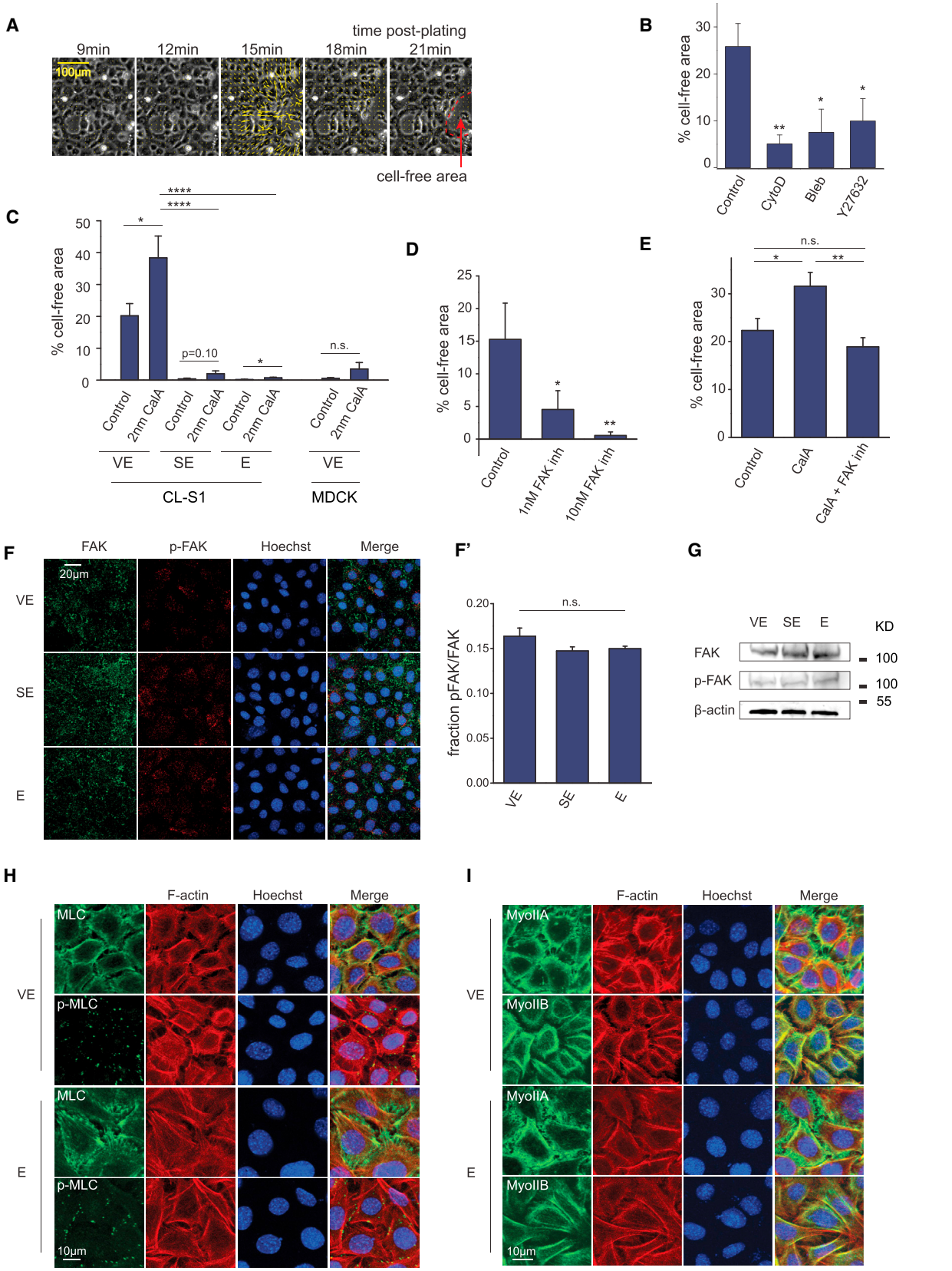

(legend on next page)

levels affected (Fig. 4 *I*). Taken together, these findings indicate that coalescence requires actomyosin contractility, and drug-induced contractility can increase coalescence on VE substrate. However, in the absence of extraneous enhancement, substrate viscoelasticity does not significantly alter levels of cellular contractility nor the apparent structural organization of the actomyosin machinery.

Substrate viscoelasticity is correlated with reorganization of vinculin and intercellular junctions

In the absence of changes in contractility and actomyosin organization, how is coalescence dependent on substrate viscoelasticity? We previously showed that CL-S1 correlated movement also depends on cadherin and others have shown that actomyosin contractility acts in concert with cadherin adhesion to generate force-induced changes in morphology (35,36). We therefore tested whether viscoelasticity-enhanced coalescence might arise from alterations in cadherin-mediated force transmission over the cellular monolayer. First, we established the localization of cadherin at cell-matrix adhesions. Although CL-S1 cells biochemically express both N-cadherin and E-cadherin (Fig. 1 *B*), at the single cell level N-cadherin is expressed in all cells, whereas E-cadherin is expressed in a subset (~10%) of cells (Fig. S2 *A*). By fluorescence microscopy, N-cadherin was more strongly and linearly localized at intercellular junctions on VE substrata, whereas its staining was weaker and more punctate on SE and E substrata (Fig. 5 *A*).

Significantly, the enhanced junctional localization of N-cadherin on VE substrate mirrored that of vinculin, which colocalized with N-cadherin on VE substrate (Fig. 5 *A*). Quantitative image analyses revealed that the proportion of junctional vinculin was significantly greater on VE than SE or E substrata (Fig. 5 *B*). To identify focal adhesions, we coimmunostained for paxillin and vinculin, and found that the proportion of vinculin that colocalized with paxillin was reduced on VE and SE substrata (Fig. 5, *C* and *D*), an indication of the relocalization of vinculin away from focal adhesions. In addition, paxillin puncta were reduced in number and size on both VE and SE substrata compared to E substrate (Fig. 5, D' and D''), demonstrating that focal adhesion number and size were affected by elasticity but not viscosity. The changes in vinculin distribution occurred without any apparent change in the total levels of N-cadherin and vinculin on the various substrata (Fig. 5 *E*). Junctional localization of vinculin on VE substrate was also increased in HeLa cells, which undergo coalescence, but was unchanged in MDCK cells, which do not undergo coalescence (Fig. S2 *B*).

We then depleted vinculin levels by siRNA transfection (Fig. 5 *F*), and the resultant cells exhibited lower levels of coalescence than control cells (Fig. 5 *G*), thus demonstrating that vinculin is necessary for the cellular response to substrate viscoelasticity. Taken together, these results show that in cell lines sensitive to substrate viscoelasticity, vinculin relocalizes from FAs to cadherin junctions, which is necessary for coalescence to occur.

Recruitment of vinculin to the cadherin complex is sufficient for viscoelasticity-induced coalescence

Vinculin is recruited to cadherin junctions by the adaptor protein α-catenin (26,37,38). To test if cadherin complexes are necessary for the junctional localization of vinculin, we depleted N-cadherin and α-catenin by siRNA transfection (Fig. 6 *A*), which resulted in significantly lower levels of coalescence (Fig. 6 *B*). Furthermore, in cells depleted of α-catenin, vinculin did not localize to junctions, but instead was concentrated in foci at the cell periphery, whereas N-cadherin was diffuse throughout the cytoplasm (Fig. 6 *C*). Image analysis showed that a significantly lower proportion of vinculin colocalized with N-cadherin in α-catenin KD cells compared to control cells (Fig. 6 C'), whereas there was no significant difference in the proportion of vinculin colocalized with paxillin (Fig. 6 C''). The proportion of junctional vinculin in α-catenin KD cells was likely an overestimate because the N-cadherin staining itself was nonjunctional. Thus, α-catenin is necessary for the recruitment of vinculin to junctional cadherin complexes in response to substrate viscoelasticity.

We hypothesized that the reduction in the FA pool of vinculin on VE substrate might be attributable to its

FIGURE 4 Coalescence is regulated by FAK-mediated actomyosin contractility. (*A*) Shown here is PIV analysis of cell movement in CL-S1 cells on VE PDMS. (*B*) CL-S1 monolayers on VE PDMS were treated with cytochalasin D (*cytoD*), blebbistatin (*Bleb*), and RhoK inhibitor Y27632, and the cell-free area was measured at 5 h postsettling ($n = 5–8$). (*C*) CL-S1 and MDCK monolayers on PDMS substrata were treated with 2 nM Calyculin A (*CalA*) or control DMSO for 2 h ($n = 5–8$). (*D*) CL-S1 monolayers on VE PDMS were treated with FAK inhibitor PF-562271 (FAK inh) and the cell-free area was measured 6 h postsettling ($n = 3–4$). (*E*) CL-S1 monolayers on VE PDMS were treated with control DMSO, 2 nM Calyculin A (*CalA*), or 2 nM CalA + 10 nM FAK inhibitor PF-562271 (*CalA + FAK inh*) ($n = 3$). (*F*) Given here are confocal images of CL-S1 cells on VE PDMS fixed and immunostained 1 h postsettling. (F') Shown here is quantitative image analysis on the levels of p-FAK relative to FAK (FAK pixels colocalized with pFAK/total FAK pixels) across different PDMS substrata (F', $n = 6–9$). (*G*) Shown here is Western blot of whole cell lysates of CL-S1 monolayers on different PDMS substrata 1 h postsettling, immunoblotted for FAK and phospho-FAK Tyr^{397} (*p-FAK*) and β-actin. (*H*) Given here are confocal projections of CL-S1 cells on different PDMS substrata fixed and immunostained for MCL/pMCL, F-actin, and nucleus, 4 h postsettling. (*I*) Confocal projections of CL-S1 cells are shown on different PDMS substrata fixed and immunostained for MyoIIA/B, F-actin, and nucleus, 4 h postsettling. *$p < 0.05$, ** < 0.01, ****$p < 0.0001$; n.s., not significant; bars represent SE. To see this figure in color, go online.

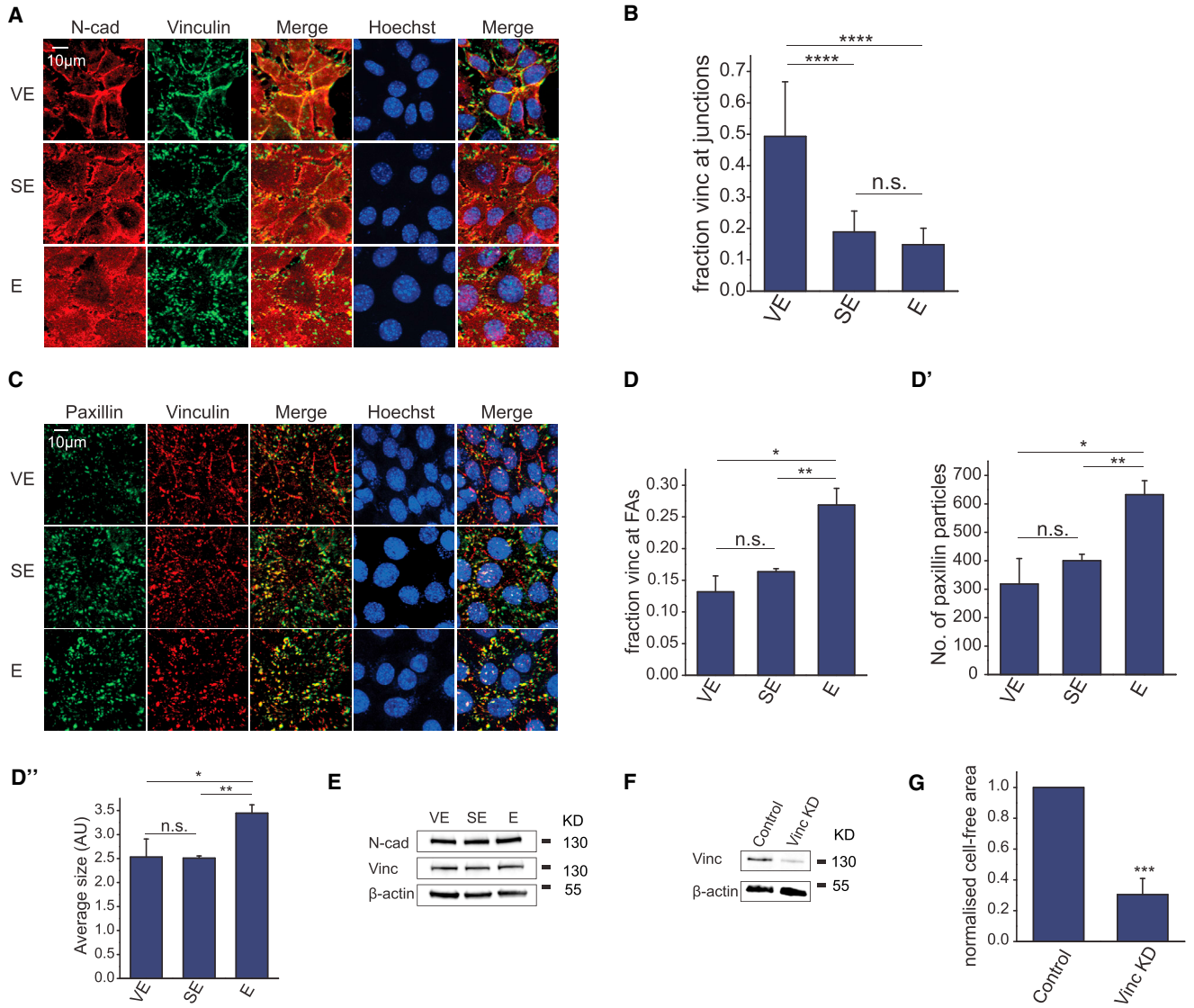

FIGURE 5 Vinculin localizes to intercellular junctions in response to substrate viscoelasticity. (*A*) Shown here are confocal projections of CL-S1 cells on different PDMS substrata fixed and immunostained for N-cadherin, vinculin, and nucleus, 4 h postsettling. N-cadherin (*N-cad*) was used as a marker of intercellular junctions. (*B*) Shown here is quantitative image analysis of vinculin localization. The fraction of junctional vinculin was calculated as the junctional intensity/total intensity ($n = 9$). (*C*) Shown here are confocal projections of CL-S1 cells on different PDMS substrata fixed and immunostained for paxillin, vinculin, and nucleus, 4 h postsettling. Paxillin was used as a marker of FAs. (*D*) Given here is quantitative image analysis of FAs. Vinculin images were segmented into FA and non-FA pools based on paxillin staining ($n = 3$). Paxillin particles were analyzed for number (*D′*) and size (*D″*) ($n = 3$–4). (*E*) Shown here is Western blot of whole cell lysates of CL-S1 monolayers harvested from different PDMS substrata immunoblotted for N-cadherin, vinculin, and *β*-actin, 6 h postsettling. (*F*) Given here is Western blot of whole cell lysates of CL-S1 cells transfected with control or vinculin (*Vinc KD*) siRNA. (*G*) Control and vinculin KD CL-S1 cells were plated on VE PDMS and the cell-free area was measured 6 h postsettling ($n = 3$). Cell-free areas of vinculin KD cells were normalized against that of control cells due to variable initial cell density after electroporation between experiments. Depletion of vinculin significantly reduced the extent of cell coalescence. $*p < 0.05$, $**p < 0.01$, $***p < 0.001$, $****p < 0.0001$; n.s., not significant; bars represent SE. To see this figure in color, go online.

decreased stability in FAs. We therefore performed FRAP analyses of GFP-vinculin in FAs on the various substrata, and found that the half-life recovery time was significantly lower on VE compared to SE and E substrata (Fig. 6 *D*), whereas the immobile fraction was unchanged across substrata (Fig. 6 *D′*). These results suggest that vinculin is less stably bound at FAs on VE substrate, which may be due to lower mechanical forces at the cell-substrate interface.

Because vinculin was necessary for coalescence in CL-S1 cells, we next investigated whether manipulation of vinculin levels would cause coalescence in MDCK cells, which do not undergo coalescence in their native state (Fig. 1, *A*, *C*, and *C′*). Indeed, MDCK cells overexpressing

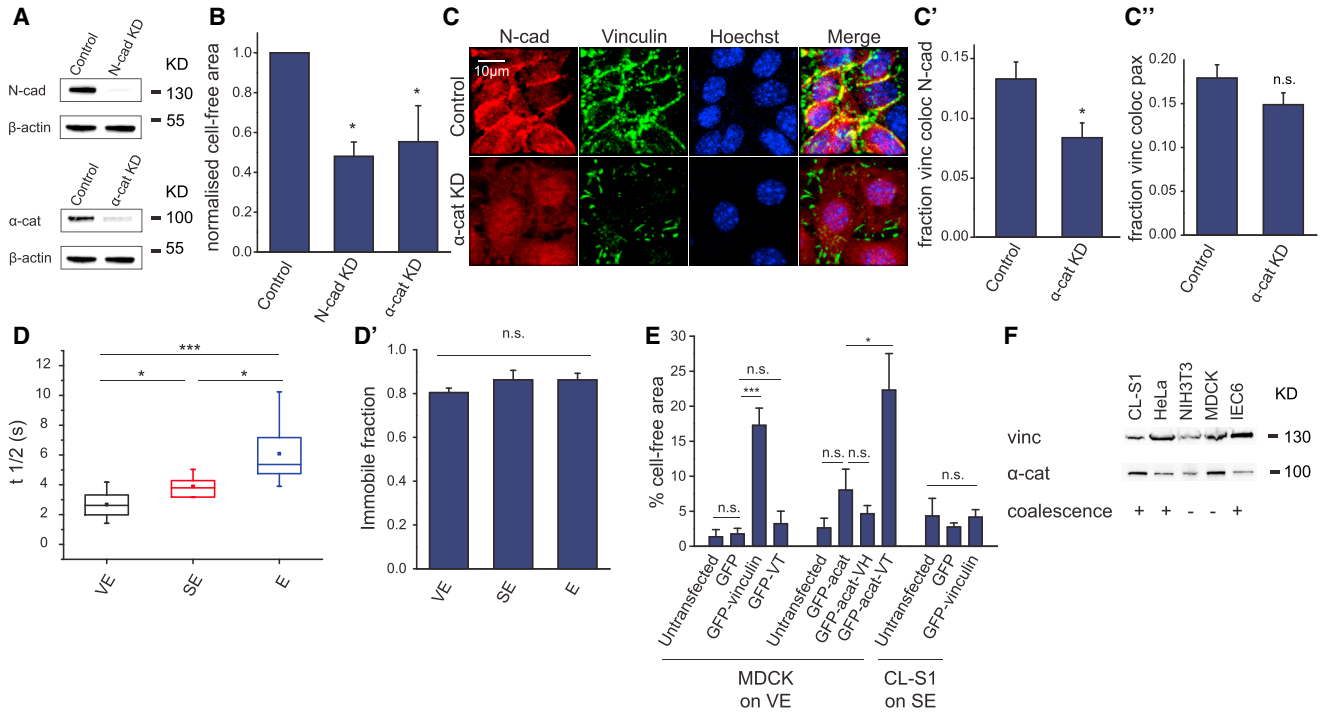

FIGURE 6 N-cadherin and α-catenin recruit vinculin to intercellular junctions. (*A*) Shown here is Western blot of whole cell lysates of CL-S1 cells transfected with control, N-cadherin (*N-cad KD*), or α-catenin (*α-cat KD*) siRNA. (*B*) Control, N-cadherin, and α-catenin KD cells were plated on VE PDMS and the cell-free area was measured 6 h postsettling ($n = 4$–7). Cell-free area of N-cad KD cells and α-cat KD were normalized against that of control cells due to variable initial cell density after electroporation between experiments. (*C*) Shown here are confocal projections of control or α-catenin KD CL-S1 monolayers on VE PDMS immunostained for N-cadherin, vinculin, and nucleus, 4 h postsettling. Quantitative image analysis is given of the proportion of vinculin colocalized with N-cadherin (*C′*, $n = 5$–6), and the proportion of vinculin colocalized with paxillin (*C″*, $n = 6$–8). (*D*) Shown here is FRAP of GFP-vinculin-expressing cells at 4–7 h postsettling on different PDMS substrata. The $t_{1/2}$ of recovery was significantly lower on VE ($n = 7$) than SE ($n = 6$) or E ($n = 11$) substrata. (*D′*) Given here are immobile fractions on different PDMS substrata. (*E*) MDCK cells overexpressing GFP, or GFP-tagged full-length vinculin (*GFP-vinculin*) or vinculin tail (*GFP-VT*) were plated on VE PDMS and the cell-free area was measured 5 h postsettling ($n = 4$). MDCK cells overexpressing GFP-tagged to amino acids 1–325 of α-Ecatenin (*GFP-αEcat*), or GFP-αEcat-tagged to the vinculin head domain (*GFP-αEcat-VH*) or tail domain (*GFP-αEcat-VT*), and untransfected cells ($n = 5$–8) were treated similarly. CL-S1 cells expressing GFP or GFP-vinculin, and untransfected cells, were plated on SE PDMS ($n = 3$). Overexpression of GFP-vinculin or GFP-αEcat-VT significantly increased cell coalescence in MDCK cells on VE PDMS, but not CL-S1 cells on SE PDMS. (*F*) Shown here is Western blot of whole cell lysates of different cell lines, immunoblotted for vinculin (*vinc*) and α-catenin (*α-cat*). Each well was loaded with the equivalent of 10% of a confluent 3.5 cm dish of cells. $*p < 0.05$, $***p < 0.001$; n.s., not significant; bars represent SE. To see this figure in color, go online.

vinculin on VE substrate underwent coalescence (Fig. 6 *E*), which shows that increased vinculin is sufficient to induce coalescence. To identify which vinculin domain was responsible for inducing coalescence, we overexpressed the vinculin head or tail domains fused to the N-terminal fragment of α-E-catenin, which binds to β-catenin and is thereby recruited to cadherin complexes. We found that the vinculin tail domain, but not the head domain, could induce coalescence in MDCK cells. This effect was dependent on its interaction with cadherin complexes, because the vinculin tail domain fused to GFP alone did not induce coalescence (Fig. 6 *E*). However, because overexpression of vinculin did not induce coalescence in CL-S1 cells on SE substrate (Fig. 6 *E*), substrate viscoelasticity is a prerequisite for vinculin to exert its effects. Moreover, Western blot analysis of cell lysates showed that protein levels of vinculin and α-catenin did not correlate with whether a particular cell type underwent viscoelasticity-induced coalescence (Fig. 6 *F*). Taken together, these data suggest that differences in total vinculin expression levels are not responsible for the cell type-dependent coalescence. Instead, each cell type may have its own threshold of vinculin expression level to respond to substrate viscoelasticity.

DISCUSSION

In vivo, the extracellular environment of the cell, and its response to mechanical stresses, are governed predominantly by the physics of viscoelasticity. Our understanding of the cellular viscous response has lagged somewhat behind that of the elastic response, perhaps due to the experimentally unwieldy nature of viscous substrata. Here, we describe, to our knowledge, a novel effect of viscoelasticity on cellular behavior: viscoelasticity-induced coalescence. In the absence of external mechanical cues,

substrate viscoelasticity was sufficient to cause coordinated and collective cellular movement in epithelial monolayers. This occurred within a short time frame of several hours, and various assays did not detect marked changes in the expression levels of key proteins or contractile activity. Therefore, it is likely that these effects arise from the rearrangement of existing proteins to redirect force transmission within the cell. Our work identified vinculin relocalization from focal adhesions to intercellular junctions as being necessary and sufficient for viscoelasticity-induced coalescence to occur.

Our most surprising finding was that the effects of viscosity and elasticity on vinculin relocalization are, to some extent, separable. The transition from the soft elastic to the viscoelastic regime was marked by a reduction in the junctional vinculin pool, without any significant change in the FA pool, whereas the converse was true for the transition between the elastic and soft elastic regime. The reduced FA pool of vinculin may be indicative of a reduction in overall FA size and number, which is a characteristic response to lower substrate elasticity (39–41). Because vinculin transfers forces between the substrate and the cytoskeleton, and drives the recruitment of key FA components including paxillin (20,28,42), it is unclear whether the reduction of vinculin at FAs is a cause or an effect of reduced FA assembly. The dependence of vinculin recruitment to FAs on substrate forces has been studied elsewhere (43), and is outside the scope of this article. What is evident from our results is that the effects on coalescence, intercellular junction reorganization, and vinculin relocalization are primarily caused by substrate viscosity, which suggests that vinculin may be a viscosity sensor in epithelial cells, acting via pathways distinct from those regulating the cellular response to elasticity.

The viscoelastic response is characterized by the localization of vinculin to cadherin complexes. Remarkably, overexpression of the vinculin tail domain was sufficient to produce viscoelasticity-induced coalescence in MDCK cells, which do not coalesce in their native state. Although we found that this coalescence was driven by actomyosin contractility, in agreement with studies of cellular aggregation on soft substrata (44), there were no evident changes in myosin II subcellular localization or activity. Instead, increased junctional vinculin may enhance linkage of the cadherin complex to the junctional actin cytoskeleton (25), which strengthens cadherin adhesion via recruitment of actin assembly regulators (24). The reinforcement of cadherin adhesion could in turn facilitate vinculin recruitment in a positive feedback cycle (25,45,46). In this way, a small shift of vinculin localization from FAs to cadherin complexes, brought upon by reduced vinculin residence times at FAs, would be sufficient to initiate vinculin redistribution and cadherin adhesion strengthening. Thus, vinculin could potentially regulate contractile forces at the intercellular junction by 1) actin reorganization via its tail domain, 2) enhancing cadherin-mediated force transmission, or 3) itself acting as a force transmitter between cadherin and actin filaments. Further studies are required to determine which of, and to what extent, these mechanisms contribute to viscoelasticity-induced coalescence.

Aside from inducing the vinculin-mediated response, substrate viscoelasticity also extended the range over which cells transmit forces through the substrate. Because substrate forces can modulate cellular motility and intercellular adhesion (11,18,47), this could be an additional mechanism by which cells could signal to neighboring cells and influence their behavior. Indeed, it has previously been shown that cells within confluent monolayers exhibit increased collective motion on soft substrate, although it should be noted that in that study the experimental timescale was on the order of several days (48). Hence, substrate viscoelasticity appears to exert its effects through a combination of biological (vinculin recruitment to intercellular junctions) and mechanical (force transmission though substrate) mechanisms.

By relocalizing between FAs and cadherin complexes in response to substrate viscoelasticity, vinculin couples the cell-matrix and cell-cell adhesion systems. A recent study has shown that force on cadherin activates phosphorylation of vinculin at Y822, which selectively drives vinculin to cell-cell junctions, where it is necessary for cadherin function (27). Here, we show that increased junctional recruitment of the vinculin tail domain could induce viscoelasticity-induced coalescence in otherwise nonresponsive MDCK cells. Taken together, these studies demonstrate that differential subcellular localization of vinculin in response to mechanical input from either cell-cell adhesions or cell-matrix adhesions can alter patterns of force transmission within the pancellular adhesion network. We speculate that shuttling of a mechanosensitive protein could transmit information about substrate viscoelasticity from the cell-matrix interface to the cell-cell interface, thus enabling cellular layers to react quickly to their mechanical environment. We expect that future extension of experiments studying cell-substrate interactions into the viscoelastic regime will provide valuable and physiologically relevant insight into adhesion signaling in large collective movements.

SUPPORTING MATERIAL

Supporting Materials and Methods, two figures, and seven movies are available at http://www.biophysj.org/biophysj/supplemental/S0006-3495(17)30853-6.

AUTHOR CONTRIBUTIONS

J.Y.Z. and S.P.H. designed and performed research, analyzed data, wrote the manuscript. Y.-J.C. designed and performed research, analyzed data, and

wrote the manuscript. A.K.Y., N.B., S.W.Z., and J.Z. contributed analytic tools. P.M. designed research, and wrote the manuscript.

ACKNOWLEDGMENTS

We thank Dr. K. H. Chiam, Dr. R. Macháň, and Dr. A. Yap for helpful feedback and suggestions. We also thank L. C. Ong, Dr. Y. Tong, and A. Paulli for technical assistance. This work was supported by a National University of Singapore (NUS) (MechanoBiology Institute; MBI) grant (R-714-001-008-271).

REFERENCES

1. Discher, D. E., P. Janmey, and Y. L. Wang. 2005. Tissue cells feel and respond to the stiffness of their substrate. *Science.* 310:1139–1143.
2. Ladoux, B., and A. Nicolas. 2012. Physically based principles of cell adhesion mechanosensitivity in tissues. *Rep. Prog. Phys.* 75: 116601.
3. Mui, K. L., C. S. Chen, and R. K. Assoian. 2016. The mechanical regulation of integrin-cadherin crosstalk organizes cells, signaling and forces. *J. Cell Sci.* 129:1093–1100.
4. Weber, G. F., M. A. Bjerke, and D. W. DeSimone. 2011. Integrins and cadherins join forces to form adhesive networks. *J. Cell Sci.* 124:1183–1193.
5. van Dam, E. A., S. D. Dams, …, F. N. van de Vosse. 2006. Determination of linear viscoelastic behavior of abdominal aortic aneurysm thrombus. *Biorheology.* 43:695–707.
6. Geerligs, M., G. W. M. Peters, …, F. P. T. Baaijens. 2008. Linear viscoelastic behavior of subcutaneous adipose tissue. *Biorheology.* 45:677–688.
7. Kasza, K. E., A. C. Rowat, …, D. A. Weitz. 2007. The cell as a material. *Curr. Opin. Cell Biol.* 19:101–107.
8. Murrell, M., R. Kamm, and P. Matsudaira. 2011. Substrate viscosity enhances correlation in epithelial sheet movement. *Biophys. J.* 101: 297–306.
9. Palacio-Torralba, J., S. Hammer, …, Y. Chen. 2015. Quantitative diagnostics of soft tissue through viscoelastic characterization using time-based instrumented palpation. *J. Mech. Behav. Biomed. Mater.* 41:149–160.
10. Cameron, A. R., J. E. Frith, and J. J. Cooper-White. 2011. The influence of substrate creep on mesenchymal stem cell behaviour and phenotype. *Biomaterials.* 32:5979–5993.
11. Cameron, A. R., J. E. Frith, …, J. J. Cooper-White. 2014. The effect of time-dependent deformation of viscoelastic hydrogels on myogenic induction and Rac1 activity in mesenchymal stem cells. *Biomaterials.* 35:1857–1868.
12. Geiger, B., J. P. Spatz, and A. D. Bershadsky. 2009. Environmental sensing through focal adhesions. *Nat. Rev. Mol. Cell Biol.* 10:21–33.
13. Rossier, O., and G. Giannone. 2016. The journey of integrins and partners in a complex interactions landscape studied by super-resolution microscopy and single protein tracking. *Exp. Cell Res.* 343:28–34.
14. Gomez, G. A., R. W. McLachlan, and A. S. Yap. 2011. Productive tension: force-sensing and homeostasis of cell-cell junctions. *Trends Cell Biol.* 21:499–505.
15. Hoffman, B. D., and A. S. Yap. 2015. Towards a dynamic understanding of cadherin-based mechanobiology. *Trends Cell Biol.* 25:803–814.
16. Leckband, D. E., and J. de Rooij. 2014. Cadherin adhesion and mechanotransduction. *Annu. Rev. Cell Dev. Biol.* 30:291–315.
17. Han, M. K. L., and J. de Rooij. 2016. Converging and unique mechanisms of mechanotransduction at adhesion sites. *Trends Cell Biol.* 26:612–623.
18. Maruthamuthu, V., B. Sabass, …, M. L. Gardel. 2011. Cell-ECM traction force modulates endogenous tension at cell-cell contacts. *Proc. Natl. Acad. Sci. USA.* 108:4708–4713.
19. Burute, M., and M. Thery. 2012. Spatial segregation between cell-cell and cell-matrix adhesions. *Curr. Opin. Cell Biol.* 24:628–636.
20. Carisey, A., R. Tsang, …, C. Ballestrem. 2013. Vinculin regulates the recruitment and release of core focal adhesion proteins in a force-dependent manner. *Curr. Biol.* 23:271–281.
21. Dumbauld, D. W., and A. J. García. 2014. A helping hand: how vinculin contributes to cell-matrix and cell-cell force transfer. *Cell Adhes. Migr.* 8:550–557.
22. Ziegler, W. H., R. C. Liddington, and D. R. Critchley. 2006. The structure and regulation of vinculin. *Trends Cell Biol.* 16:453–460.
23. Case, L. B., M. A. Baird, …, C. M. Waterman. 2015. Molecular mechanism of vinculin activation and nanoscale spatial organization in focal adhesions. *Nat. Cell Biol.* 17:880–892.
24. Leerberg, J. M., G. A. Gomez, …, A. S. Yap. 2014. Tension-sensitive actin assembly supports contractility at the epithelial zonula adherens. *Curr. Biol.* 24:1689–1699.
25. Thomas, W. A., C. Boscher, …, S. Dufour. 2013. α-Catenin and vinculin cooperate to promote high E-cadherin-based adhesion strength. *J. Biol. Chem.* 288:4957–4969.
26. Yonemura, S., Y. Wada, …, M. Shibata. 2010. α-Catenin as a tension transducer that induces adherens junction development. *Nat. Cell Biol.* 12:533–542.
27. Bays, J. L., X. Peng, …, K. A. DeMali. 2014. Vinculin phosphorylation differentially regulates mechanotransduction at cell-cell and cell-matrix adhesions. *J. Cell Biol.* 205:251–263.
28. Goldmann, W. H. 2016. Role of vinculin in cellular mechanotransduction. *Cell Biol. Int.* 40:241–256.
29. Maddugoda, M. P., M. S. Crampton, …, A. S. Yap. 2007. Myosin VI and vinculin cooperate during the morphogenesis of cadherin cell-cell contacts in mammalian epithelial cells. *J. Cell Biol.* 178:529–540.
30. Preibisch, S., S. Saalfeld, and P. Tomancak. 2009. Globally optimal stitching of tiled 3D microscopic image acquisitions. *Bioinformatics.* 25:1463–1465.
31. Petitjean, L., M. Reffay, …, P. Silberzan. 2010. Velocity fields in a collectively migrating epithelium. *Biophys. J.* 98:1790–1800.
32. Vedula, S. R. K., M. C. Leong, …, B. Ladoux. 2012. Emerging modes of collective cell migration induced by geometrical constraints. *Proc. Natl. Acad. Sci. USA.* 109:12974–12979.
33. Seo, J. H., K. Sakai, and N. Yui. 2013. Adsorption state of fibronectin on poly(dimethylsiloxane) surfaces with varied stiffness can dominate adhesion density of fibroblasts. *Acta Biomater.* 9:5493–5501.
34. Dumbauld, D. W., H. Shin, …, A. J. García. 2010. Contractility modulates cell adhesion strengthening through focal adhesion kinase and assembly of vinculin-containing focal adhesions. *J. Cell. Physiol.* 223:746–756.
35. Martin, A. C., M. Gelbart, …, E. F. Wieschaus. 2010. Integration of contractile forces during tissue invagination. *J. Cell Biol.* 188:735–749.
36. Vasquez, C. G., and A. C. Martin. 2016. Force transmission in epithelial tissues. *Dev. Dyn.* 245:361–371.
37. Ladoux, B., W. J. Nelson, …, R. M. Mège. 2015. The mechanotransduction machinery at work at adherens junctions. *Integr. Biol.* 7:1109–1119.
38. Maki, K., S.-W. Han, …, T. Adachi. 2016. Mechano-adaptive sensory mechanism of α-catenin under tension. *Sci. Rep.* 6:24878.
39. Balaban, N. Q., U. S. Schwarz, …, B. Geiger. 2001. Force and focal adhesion assembly: a close relationship studied using elastic micropatterned substrates. *Nat. Cell Biol.* 3:466–472.
40. Gupta, M., B. R. Sarangi, …, B. Ladoux. 2015. Adaptive rheology and ordering of cell cytoskeleton govern matrix rigidity sensing. *Nat. Commun.* 6:7525.
41. Trichet, L., J. Le Digabel, …, B. Ladoux. 2012. Evidence of a large-scale mechanosensing mechanism for cellular adaptation to substrate stiffness. *Proc. Natl. Acad. Sci. USA.* 109:6933–6938.
42. Dumbauld, D. W., T. T. Lee, …, A. J. García. 2013. How vinculin regulates force transmission. *Proc. Natl. Acad. Sci. USA.* 110:9788–9793.
43. Yu, C. H., J. B. K. Law, …, M. P. Sheetz. 2011. Early integrin binding to Arg-Gly-Asp peptide activates actin polymerization and contractile

movement that stimulates outward translocation. *Proc. Natl. Acad. Sci. USA.* 108:20585–20590.

44. Guo, W. H., M. T. Frey, …, Y. L. Wang. 2006. Substrate rigidity regulates the formation and maintenance of tissues. *Biophys. J.* 90:2213–2220.
45. le Duc, Q., Q. Shi, …, J. de Rooij. 2010. Vinculin potentiates E-cadherin mechanosensing and is recruited to actin-anchored sites within adherens junctions in a myosin II-dependent manner. *J. Cell Biol.* 189:1107–1115.
46. Dufour, S., R.-M. Mège, and J. P. Thiery. 2013. α-Catenin, vinculin, and F-actin in strengthening E-cadherin cell-cell adhesions and mechanosensing. *Cell Adhes. Migr.* 7:345–350.
47. Ladoux, B., E. Anon, …, R. M. Mège. 2010. Strength dependence of cadherin-mediated adhesions. *Biophys. J.* 98:534–542.
48. Angelini, T. E., E. Hannezo, …, D. A. Weitz. 2010. Cell migration driven by cooperative substrate deformation patterns. *Phys. Rev. Lett.* 104:168104.